

Submitted *The Astronomical Journal*

## The Motions of Clusters of Galaxies and the Dipoles of the Peculiar Velocity Field

Riccardo Giovanelli, Martha P. Haynes

Center for Radiophysics and Space Research and National Astronomy and Ionosphere Center<sup>1</sup>, Cornell University, Ithaca, NY 14853

John J. Salzer

Astronomy Dept., Wesleyan University, Middletown, CT 06459

Gary Wegner

Dept. of Physics and Astronomy, Dartmouth College, Hanover, NH 03755

Luiz N. da Costa

European Southern Observatory, Karl-Schwarzschild-Str. 2, D-85748 Garching b. München, Germany and Observatorio Nacional, Rio de Janeiro, Brazil

Wolfram Freudling

Space Telescope-European Coordinating Facility and European Southern Observatory, Karl-Schwarzschild-Str. 2, D-85748 Garching b. München, Germany

### ABSTRACT

In preceding papers of this series, TF relations for galaxies in 24 clusters with radial velocities between 1000 and 9200 km s<sup>-1</sup> (SCI sample) were obtained, a Tully-Fisher (TF) template relation was constructed and mean offsets of each cluster with respect to the template obtained. Here, an estimate of the line-of-sight peculiar velocities of the clusters and their associated errors are given. It is found that cluster peculiar velocities in the Cosmic Microwave Background reference frame do not exceed 600 km s<sup>-1</sup> and that their distribution has a line-of-sight dispersion of 300 km s<sup>-1</sup>, suggesting a more quiescent cluster peculiar velocity field than previously reported. When measured in a reference frame in which the Local Group is at rest, the set of clusters at  $cz > 3000$

---

<sup>1</sup>The National Astronomy and Ionosphere Center is operated by Cornell University under a cooperative agreement with the National Science Foundation.

km s<sup>-1</sup> exhibits a dipole moment in agreement with that of the CMB, both in amplitude and apex direction. It is estimated that the bulk flow of a sphere of 6000 km s<sup>-1</sup> radius in the CMB reference frame is between 140 and 320 km s<sup>-1</sup>.

*Subject headings:* galaxies: distances and redshifts – cosmology: observations; cosmic microwave background; distance scale

## 1. Introduction

The Cosmic Microwave Background (CMB) radiation dipole moment is generally interpreted as a Doppler shift resulting from the motion of the Sun with respect to the comoving reference frame. The vector associated with that motion has an amplitude of  $368.7 \pm 2.5$  km s<sup>-1</sup>, and is directed toward  $l = 264.31^\circ \pm 0.16$ ,  $b = +48.05^\circ \pm 0.09$  (Lineweaver *et al.* 1996). Allowing for solar motion with respect to the Local Standard of Rest, rotation of the Local Standard of Rest about the galactic center and motion of the Galaxy with respect to the center of mass of the Local Group (LG) of galaxies (motions known with increasing absolute uncertainty), the CMB dipole translates into a velocity  $\mathbf{V}_{cmb}$  of the LG with respect to the comoving reference frame, of amplitude  $611 \pm 22$  km s<sup>-1</sup> and directed towards  $l = 273^\circ \pm 3^\circ$ ,  $b = 27^\circ \pm 3^\circ$ . Most of the uncertainty in the latter vector arises from that on the motion of the Sun with respect to the LG, which we assume to have an amplitude of 300 km s<sup>-1</sup> and directed towards  $l = 90^\circ$ ,  $b = 0^\circ$  (de Vaucouleurs, de Vaucouleurs & Corwin 1976)<sup>2</sup>.

In linear theory, the peculiar velocity induced on the LG by the inhomogeneities present within a sphere of radius  $R$  is

$$\mathbf{V}_{pec, LG}(R) = \frac{H_o \Omega_o^{0.6}}{4\pi} \int \delta_{mass}(\mathbf{r}) \frac{\mathbf{r}}{r^3} W(r, R) d^3\mathbf{r} \quad (1)$$

---

<sup>2</sup>Several solutions of the solar motion with respect to the LG exist. When expressed in terms of their Cartesian components — directed respectively towards the Galactic Center,  $(l, b) = (90^\circ, 0^\circ)$  and  $b = 90^\circ$  —, the most frequently used solutions are respectively (i): (0, 300, 0) (De Vaucouleurs *et al.* 1976), (ii): (-79, 295, -38) (Yahil, Sandage & Tammann 1977) and (iii): (-30, 297, -27) (Lynden-Bell & Lahav 1988), with units in km s<sup>-1</sup>. They agree within the accuracies with which each is determined, and we follow Lynden-Bell & Lahav’s suggestion to adopt the easy-to-remember solution (i), for the sake of standardization and simplicity. The vector differences of the Lineweaver *et al.* (1996) dipole and the above mentioned solutions yield estimates of the the LG motion with respect to the CMB. They are, respectively, (i): (-24, -545, 274) or 611 km s<sup>-1</sup> towards  $(l, b) = (273^\circ, +27^\circ)$ ; (ii): (55, -540, 312) or 626 km s<sup>-1</sup> towards  $(l, b) = (276^\circ, +30^\circ)$  and (iii): (6, -542, 301) or 620 km s<sup>-1</sup> towards  $(l, b) = (271^\circ, +29^\circ)$ .

where  $W(r, R)$  is a window function of width  $R$ ,  $H_0 \mathbf{r}$  is the distance in  $\text{km s}^{-1}$ ,  $\delta_{mass}$  is the mass overdensity at  $\mathbf{r}$  and  $\Omega_0$  is the cosmological density parameter. If the CMB dipole is the result of a Doppler shift, as we will assume in the remainder of this paper, then there must be identity between  $\mathbf{V}_{cmb}$  and  $\mathbf{V}_{pec,LG}(R)$  as  $R \rightarrow \infty$ . Direct measurements of the peculiar velocity field of galaxies and clusters allow us such a comparison. They also allow an estimate of the *convergence depth* of the local Universe. The integral in Equation (1) converges in the measure in which the average value of  $\delta_{mass}$  within a shell of radius  $R$  approaches zero, as  $R$  increases. In a universe which on large scales is homogeneous, the convergence depth is approached at scales several times larger than the correlation scalelength. In a fractal universe, the issue is more complex (Pietronero *et al.* 1997; Guzzo 1998). We define the convergence depth  $d_c$  as the distance at which first  $\mathbf{V}_{pec,LG}(R) = \mathbf{V}_{cmb}$ , within the errors. Because  $\mathbf{V}_{pec,LG}(R)$  may oscillate before settling on an asymptotic value, as suggested by the results of Hudson (1993), Strauss *et al.* (1992), Scaramella *et al.* (1994), Tini–Brunozzi *et al.* (1995) and Branchini *et al.* (1996), among others, the concept of convergence depth is somewhat ambiguous. Nonetheless, since the radius sampled by the clusters in the sample discussed in this paper is larger than the correlation length of the galaxian population as obtained from redshift surveys, it is legitimate to ask whether the peculiar velocity induced by the large–scale distribution of matter they trace approaches  $\mathbf{V}_{cmb}$ . In other words, is convergence reached within the largest scale sampled by the cluster sample?

The first attempt to measure the large scale motion of the LG was carried out by Rubin *et al.* (1976). For an all–sky sample of 96 Sc I galaxies enclosed in the redshift shell bound by 3500 and 6500  $\text{km s}^{-1}$ , they measured the dipole of the quantity  $HM = \log(cz) - 0.2m$ , where  $z$  is the redshift,  $m$  the galaxy’s apparent magnitude and  $c$  the speed of light. The derived dipole suggested a LG motion of  $454 \pm 125 \text{ km s}^{-1}$  towards  $(l_{ScI}, b_{ScI}) = (163^\circ, -11^\circ)$ , significantly discrepant with that indicated by  $\mathbf{V}_{cmb}$ , which was measured soon thereafter.

Virgocentric infall (as recently redetermined by Jerjen & Tammann 1993), contributes only a fraction of the motion of the LG. The amplitude of the LG infall towards Virgo, which is directed about  $45^\circ$  away from  $\mathbf{V}_{cmb}$ , is on the order of  $200 \text{ km s}^{-1}$ . Shaya (1984) and Tammann & Sandage (1985) suggested that the Hydra–Centaurus supercluster, at a redshift of 3–4000  $\text{km s}^{-1}$ , or supercluster structures obscured in the Zone of Avoidance (ZoA), played a more important role than Virgo in determining the peculiar velocity of the LG. This suggestion found confirmation in the analysis of Lynden–Bell *et al.* (1988), who proposed the existence of a “Great Attractor” (GA) located at 4350  $\text{km s}^{-1}$  and very close to the galactic plane. Applications of the *Potent* method yield density field reconstructions which, albeit grossly smoothed, exhibit a broad density peak near  $(l_{ga}, b_{ga}) = (320^\circ, 0^\circ)$  at 4000  $\text{km s}^{-1}$  (Dekel 1994; da Costa *et al.* 1996). In 1989, Scaramella *et al.* pointed out the

directional coincidence between the GA and the Shapley Supercluster, a large concentration of clusters near  $cz \sim 14000 \text{ km s}^{-1}$ , hypothesizing that infall towards such distant structure is an important component of the local peculiar velocity field. This result was echoed by the interpretations of Willick (1990) and Mathewson *et al.* (1992) and disputed by Dressler & Faber (1990). More recently, Lauer & Postman (1994) reported that the LG motion with respect to the reference frame defined by a sample of 119 clusters of galaxies extending to  $cz \sim 15000 \text{ km s}^{-1}$  can be represented by a vector  $\mathbf{V}_{lp}$  of amplitude  $561 \pm 284 \text{ km s}^{-1}$ , directed towards  $(l, b) = (220^\circ, -28^\circ) \pm 27^\circ$ . The large discrepancy between  $\mathbf{V}_{lp}$  and  $\mathbf{V}_{cmb}$  was interpreted as due to an overall bulk flow of the cluster reference frame of  $689 \pm 178 \text{ km s}^{-1}$  towards  $(l, b) = (343^\circ, +53^\circ)$ . The dynamical implication of this result, which was confirmed by neither Riess *et al.* (1995) nor Giovanelli *et al.* (1996), is that the LG motion and that of the Lauer & Postman cluster sample are caused *largely* by mass concentrations beyond  $15,000 \text{ km s}^{-1}$ , thus postulating a very large, or altogether absence of, local convergence depth.

This paper is part of a series based on spectroscopy and I band photometry of spiral galaxies, obtained with the purpose of improving the calibration of the Tully–Fisher relation (Tully and Fisher 1977) and our understanding of the peculiar velocity field in the local universe. Previous papers in the series are listed in Giovanelli *et al.* (1997a,b, hereafter Papers VI and VII). In Paper VI we presented a set of galaxy TF parameters in cluster fields (SCI sample), and in Paper VII we obtained a template TF relation by combining the cluster data. The general motivations for those studies are given in the introduction of Paper VI.

The main goal of this paper is to investigate the large–scale deviations from Hubble flow, as traced by the clusters of galaxies introduced in Papers VI and VII. Although the set includes only 24 clusters, their peculiar velocities are derivable with relatively high accuracy. The analysis we carry out is simple and, in comparison with that made with samples of field galaxies, its results require much smaller corrections for observational biases. Analogous studies have been carried out in the past (e.g. Mould *et al.* 1991), but with data of inferior accuracy (see Scodreggio 1997). Due to the sparse sampling provided by clusters, the results of this study do not provide a detailed description of the peculiar velocity field. However, they can yield a good estimate of its dipole moment and allow a direct comparison with  $\mathbf{V}_{cmb}$ .

It is well known that the estimate of peculiar velocities via the TF relation is independent on the assumed value of the Hubble constant  $H_0$ . The technique does however need careful calibration in order for the *velocity zero point* to be established. The template relation obtained by us in Paper VII provides such calibration. In that work, we also

estimated the departure in magnitudes of each cluster TF relation from the template relation, after correction for a number of biases that arise in this type of analysis. If the calibration of the template relation is correct, the magnitude offset of each cluster can be combined with its systemic velocity to estimate a peculiar velocity. In Section 2, we thus estimate cluster motions. If the calibration of the TF template relation is incorrect, a geocentric component in the derived peculiar velocity field is introduced, simulating either global expansion or contraction. This would not alter the dipole signature of the peculiar velocity field but the individual velocities would be obviously incorrect. In Section 3 we discuss the accuracy of our template relation and thus estimate the degree to which our TF template relation can be globally assumed to define rest with respect to the comoving reference frame. In Section 4 we discuss the global motion of such large-scale structures as the Pisces–Perseus supercluster (PP) and the Hydra–Centaurus supercluster (HC). In Section 5 we inspect the incompleteness of our cluster sample and discuss its impact on the derivation of dipole parameters. In Section 6, we derive the cluster peculiar velocity distribution function. In Section 7 we compute the dipole moment of the cluster peculiar velocity field and investigate the amplitude of bulk flows in the local universe. A summary of our results is presented in Section 8.

## 2. Cluster Motions

In Paper VI, we presented the TF parameters of the SCI sample of galaxies in 24 clusters. The clusters are well distributed over the sky and extend to a maximum  $cz \sim 9200$  km s<sup>-1</sup>. The relevant cluster parameters are given in Table 1 of Paper VI, while the galaxy data are listed in Table 2, *ibidem*. Cluster membership was assigned to each galaxy in the sample on the basis of criteria that were more stringent than generally adopted in previous TF work. The photometric observations were all carried out in the I band.

Galaxies associated with each cluster are separated into two classes: (i) the **in** sample includes galaxies that are very likely cluster members, on the basis of their sky and redshift coordinates; (ii) a class of “peripheral” galaxies is characterized by redshift quite close to the systemic one of the cluster, but sufficiently removed spatially from the cluster center so that a membership assignment cannot be reliably made. The combination of **in** and peripheral objects for a given cluster is referred to as the **in+** sample. The SCI **in** sample of the 24 clusters includes 374 galaxies, of which 360 are deemed good candidates for TF work, while the SCI **in+** sample includes 584 objects, of which 555 are used for TF work. The remaining 198 galaxies for which TF parameters were presented in Paper VI are either foreground or background objects, or members of inadequately sampled groups/clusters.

Table 1. Cluster Motions

| Cluster    | $\langle \Delta m \rangle$<br><b>in</b> | $\langle \Delta m \rangle$<br><b>in+</b> | $cZ_{hel}$ | $cZ_{LG}$ | $cZ_{cmb}$ | $V_{tf,cmb}$<br><b>in</b> | $V_{pec,cmb}$<br><b>in</b> | $V_{tf,cmb}$<br><b>in+</b> |
|------------|-----------------------------------------|------------------------------------------|------------|-----------|------------|---------------------------|----------------------------|----------------------------|
| (1)        | (2)                                     | (3)                                      | (4)        | (5)       | (6)        | (7)                       | (8)                        | (9)                        |
| N383       | −0.027(126)                             | +0.003(076)                              | 5161(032)  | 5368      | 4865       | 4805                      | +60(279)                   | 4871                       |
| N507       | −0.112(111)                             | −0.043(094)                              | 5091(099)  | 5291      | 4808       | 4566                      | +242(233)                  | 4714                       |
| A262       | +0.015(085)                             | −0.033(063)                              | 4918(080)  | 5105      | 4664       | 4696                      | −32(+184)                  | 4594                       |
| A400       | +0.077(111)                             | +0.039(070)                              | 7142(075)  | 7178      | 6934       | 7184                      | −250(367)                  | 7060                       |
| Eridanus   | +0.433(116)                             | +0.393(087)                              | 1665(030)  | 1567      | 1534       | 1872                      | −338(100)                  | 1838                       |
| Fornax     | +0.053(098)                             | +0.173(090)                              | 1415(045)  | 1266      | 1321       | 1354                      | −33(061)                   | 1430                       |
| Cancer     | −0.113(092)                             | −0.027(077)                              | 4705(080)  | 4604      | 4939       | 4689                      | +250(198)                  | 4878                       |
| Antlia     | −0.128(107)                             | −0.133(080)                              | 2800(100)  | 2517      | 3120       | 2941                      | +179(145)                  | 2935                       |
| Hydra      | +0.236(080)                             | +0.164(070)                              | 3733(050)  | 3465      | 4075       | 4542                      | −467(167)                  | 4395                       |
| N3557      | −0.052(136)                             | −0.134(108)                              | 3000(070)  | 2726      | 3318       | 3239                      | +79(203)                   | 3119                       |
| A1367      | −0.014(065)                             | −0.020(062)                              | 6408(088)  | 6336      | 6735       | 6692                      | +43(200)                   | 6673                       |
| Ursa Major | +0.687(080)                             | +0.710(080)                              | 896(040)   | 965       | 1101       | 1511                      | −410(056)                  | 1526                       |
| Cen30      | −0.138(098)                             | −0.213(070)                              | 3041(150)  | 2805      | 3322       | 3117                      | +205(140)                  | 3012                       |
| A1656      | −0.052(065)                             | −0.065(058)                              | 6917(068)  | 6926      | 7185       | 7015                      | +170(210)                  | 6973                       |
| ESO508     | −0.382(185)                             | −0.302(100)                              | 2900(100)  | 2720      | 3210       | 2693                      | +517(230)                  | 2793                       |
| A3574      | +0.073(165)                             | +0.012(078)                              | 4548(030)  | 4374      | 4817       | 4982                      | −165(379)                  | 4843                       |
| A2197†     | +0.066(160)                             | +0.048(090)                              | 9138(100)  | 9334      | 9162       | 9444                      | −282(693)                  | 9285                       |
| A2199†     | +0.056(160)                             | +0.048(090)                              | 8970(098)  | 9163      | 8996       | 9231                      | −235(681)                  | 9285                       |
| Pavo II    | −0.118(175)                             | −0.068(082)                              | 4470(070)  | 4342      | 4444       | 4209                      | +235(339)                  | 4307                       |
| Pavo       | −0.108(225)                             | −0.043(120)                              | 4100(100)  | 3952      | 4055       | 3858                      | +197(400)                  | 3975                       |
| MDL59      | +0.487(180)                             | +0.427(092)                              | 2590(075)  | 2636      | 2317       | 2900                      | −583(240)                  | 2820                       |
| Pegasus    | +0.032(126)                             | +0.112(105)                              | 3888(080)  | 4087      | 3519       | 3571                      | −52(207)                   | 3705                       |
| A2634‡     | +0.020(070)                             | +0.033(065)                              | 9240(079)  | 9484      | 8895       | 8977                      | −82(289)                   | 9031                       |
| A2666      | +0.043(127)                             |                                          | 8118(081)  | 8357      | 7776       | 7931                      | −156(459)                  |                            |

†Parms. for **in+** samples include A2197, A2199 and peripheral objects.

‡Uses expanded sample of Scodreggio, Giovanelli and Haynes (1997).

In Paper VII, the cluster data were combined to obtain a template TF relation. This was done separately for the **in** and for the **in+** objects. To that end, the subset of 14 clusters with  $cz > 4000 \text{ km s}^{-1}$  was assumed to yield a null average peculiar velocity. This is equivalent to setting equal to zero the amplitude of any *geocentric* global deviation from Hubble flow for the spherical shell between 4000 and 9200  $\text{km s}^{-1}$ , and translates into the definition of a zero point of the template TF relation. Magnitude offsets  $\Delta m$  of each cluster with respect to that template can be converted into peculiar velocities via the relation

$$V_{pec,cmb} = cz_{cmb}(1 - 10^{0.2\Delta m}) \quad (2)$$

where  $cz_{cmb}$  is the cluster systemic velocity with respect to the CMB reference frame and  $V_{pec,cmb}$  is the cluster peculiar velocity, in the same reference frame.

In Table 1, we list the mean magnitude offsets  $\Delta m$ , computed separately for each (**in**) and each (**in+**) cluster sample, respectively in columns 2 and 3. Those offsets are derived as

$$\Delta m = (1/4) \sum_{i=1}^4 \Delta y_i, \quad (3)$$

where the  $\Delta y_i$  are the magnitude offsets listed in columns 4–7 of Table 3 of Paper VII; the four  $\Delta y_i$ 's were estimated for two different slopes of the faint end of the galaxy luminosity function (each leading to different incompleteness bias corrections for the various cluster samples) and for both a linear and a quadratic fit to the TF template relation. The four solutions differ slightly, by amounts generally smaller than the typical uncertainty. An equal-weight average of the four offsets is adopted here. The uncertainty on  $\Delta m$ ,  $\epsilon_\mu$ , is listed in parenthesized form in Table 1: i.e.  $-0.027(126)$  is equivalent to  $-0.027 \pm 0.126$ .  $\epsilon_\mu$  is an error on the TF distance modulus and the cumulative result of the uncertainties arising from:

- (i) the number of galaxies and the quality of their TF parameters in each cluster sample;
- (ii) the TF template relation parameters, both those deriving from the formal fits and those associated with systematic effects, as gauged in Paper VII, Section 6;
- (iii) the cluster incompleteness bias correction (see Paper VII, Section 6.3);
- (iv) the measured systemic velocity of each cluster;
- (v) the quality of the kinematical zero point, obtained by assuming that the mean peculiar velocity of clusters at  $cz_{cmb} > 4000 \text{ km s}^{-1}$  is zero, as described in Section 6.2 of Paper VII.

The values  $\epsilon_\mu$  listed in Table 1 are conservative, erring more likely toward an overestimate of the uncertainties, except for an important proviso. The uncertainty arising from the

quality of the kinematical zero point, mentioned in (v) above, is derived from the amplitude of the cluster peculiar velocity distribution function and on the number of objects used, on the assumption that the mean peculiar velocity of distant clusters is zero, i.e. that there is no large-scale geocentric signature in the peculiar velocity field. If however the LG were to be located near the center of a large-scale, isotropic void or positive density enhancement, an acceleration or delay of the Hubble expansion would take place, and the peculiar velocity field would have a geocentric signature. We discuss this possibility in Section 3. For the moment, we assume that such a signature is of negligible amplitude.

Other contents of Table 1 include: the systemic velocity of the cluster in the solar, Local Group and CMB reference frame (columns 4, 5 and 6); the peculiar velocities measured in the CMB reference frame for each cluster, respectively for the **in** (column 8) and the **in+** (column 10) samples; the TF distance of the cluster, expressed in  $\text{km s}^{-1}$ , i.e.

$$cz_{tf,cmb} = cz_{cmb} - V_{pec,cmb} \quad (4)$$

is tabulated for the **in** sample in column 7 and the **in+** sample in column 9. Peculiar velocities and TF distances in Table 1 are not corrected for the Malmquist bias, which is discussed in Section 6. Errors on the systemic and peculiar velocities of the clusters are given in parenthesized form in columns 4, 8 and 10. Errors on the peculiar velocities, inferred from  $\epsilon_\mu$ , are actually slightly asymmetric about the mean value adopted; for example,  $\Delta m = +0.015 \pm 0.085$  for the **in** sample of A262 translates into  $V_{pec,cmb} = -32_{-188}^{+180}$ . In Table 1, we list the uncertainty on  $V_{pec,cmb}$  as the mean of the upper and lower side errors.

Note that in the case of the clusters A2197 and A2199, a single **in+** sample is adopted, which includes both clusters, very close in redshift to each other, and their peripheries. For A2666, no **in+** sample is defined, due to the confusing nearness in projection of A2634.

For A2634, rather than the samples described in Paper VII we use those presented by Scodreggio, Giovanelli & Haynes (1997), which include additional objects, unavailable for the Paper VII study. The expansion of the A2634 sample size by approximately one third leads to a revision of the average magnitude offset, with respect to the TF template relation, of  $-0.035$  mag, in comparison to the Paper VII result, a change amounting to about  $(1/2)\epsilon_\mu$ .

A few interesting details of Table 1 are worth underscoring. First, no values of the cluster line-of-sight peculiar velocity are measured, in excess of  $\pm 600 \text{ km s}^{-1}$ , in the CMB reference frame. Second, the largest velocities are measured for nearby groups, structures within  $cz \sim 3000 \text{ km s}^{-1}$  from the Local Group. This overall relatively quiescent picture of the peculiar velocity field is in marked contrast of previous cluster peculiar velocity measurements. The comparison between the peculiar velocities obtained from spiral and elliptical samples for a single cluster, as shown in Mould *et al.* (1991) was



until recently discouragingly poor, suggesting that the large amplitude of the estimated peculiar velocities resulted from systematic errors unaccounted for by the reported scatter in the TF or Fundamental Plane techniques. The situation has improved significantly, and recent comparisons exhibit very noticeably reduced scatter, a higher degree of correlation and much reduced amplitude in the peculiar velocities inferred, as shown by Scodreggio, Giovanelli & Haynes (1998).

### 3. Does the TF Template Relation Represent a Rest Reference Frame?

The TF relation is a linear function relating the logarithm of a galaxy’s velocity width and its absolute magnitude:

$$M = a + b(\log W - 2.5). \quad (5)$$

In paper VII, we estimated the total uncertainty on  $a$  to be on the order of 0.05 mag, arising mostly from the limits on our ability to characterize the ensemble of clusters with  $cz_{tf} > 4000 \text{ km s}^{-1}$  as a good approximation to a comoving reference frame. The uncertainty on the slope  $b$  is on the order of 2%.

An error on the zero point  $a$  of the TF template relation translates into the spurious generation of a geocentric peculiar velocity field, of amplitude which increases linearly with distance. In other words, it simulates an isotropic distortion  $\delta H$  of the Hubble expansion. An error of 0.05 mag in  $a$  simulates a slowdown or speeding up of the Hubble expansion by 2.3%.

An error on the slope  $b$  also translates in an isotropic, spurious distortion of the Hubble flow. The distortion does however affect near and distant sources in different ways. If  $a$  is correct and  $b$  is too steep, for example, galaxies of large width will tend to have positive magnitude offsets  $\Delta m$  with respect to (4), i.e. negative peculiar velocities, while the opposite will be true for galaxies of velocity width  $\log W < 2.5$ . Most TF samples span a large range of distances. At some distance  $d_e$  within that range, galaxies of large width may be as likely to be members of the sample as galaxies of small width. The error in  $b$  would then produce a spurious acceleration of the Hubble flow at  $d < d_e$  and a spurious deceleration at  $d > d_e$ .

These effects are easily spotted in all-sky surveys, while in surveys that concentrate on selected parts of the sky, such geocentric effects are more difficult to identify and can easily be misinterpreted as the signature of bulk flows. There is however an insidious possibility that can wreak havoc even when full-sky coverage is available. If, as briefly mentioned in the preceding Section, the LG were to be located near the center of a roughly spherical,

large-scale density fluctuation, geocentric distortions of the Hubble flow would be real, rather than the result of poor parametrization of the distance determination technique. Recently, Zehavi *et al.* (1998) have suggested precisely that possibility: that the volume within  $cz \sim 7000 \text{ km s}^{-1}$  is subject to a Hubble acceleration of  $(6.6 \pm 2.2)\%$ , resulting from a local underdensity of 20%, surrounded by an overdense shell. The possibility of a large-scale geocentric peculiar velocity field was excluded by the way our template TF relation was defined. However, the Zehavi *et al.* result can in principle be tested with our data: a “Hubble bubble” can be distinguished from a distance calibration error by detecting the “edge” of the perturbed region. If present, the claimed effect would produce a differential TF offset of 0.14 mag between nearby clusters and those more distant than  $7000 \text{ km s}^{-1}$ .

In figure 1 we carry out such a test. Using the data in Table 1, we plot  $\delta H/H = V_{pec,cmb}/cz_{tf,cmb}$  against  $hd = cz_{tf,cmb}/100$  (with the implicit usual parametrization  $H_o = 100h$ ), separately for the peculiar velocities computed for the **in** and for the **in+** samples (panels *a* and *b* respectively). Inset in the figures are the average values of  $\delta H/H$  for three intervals of  $hd$ : 30 to 60, 35 to 60 and 60 to 95 Mpc. At small distances, the peculiar velocity field is quite unstable, dominated by the large velocities of nearby groups, which are comparable to those of the LG ( $611 \text{ km s}^{-1}$ ) and constitute a significant fraction of the Hubble flow. At distances larger than  $35h^{-1}$  Mpc, the monopole of the cluster velocity field does not exhibit significant change of value, the Hubble flow at  $hd > 60$  Mpc appearing to differ from that between 30 and 60 Mpc by less than 3%, rather than the 6.6% reported by Zehavi from their SNe Ia sample. The results shown in Figure 1 should however be considered inconclusive, as the redshift range of our sample is about three times smaller than that of the SNe Ia, and our cluster sample barely straddles the edge of the purported change of regime on the Hubble flow. The small number of clusters farther than  $70h^{-1}$  Mpc allows for cosmic variance to mask the effect of a change in the Hubble flow. While our data do not corroborate the claim of Zehavi *et al.*, neither do they refute it. A more thorough check of the Zehavi *et al.* hypothesis will be possible soon, as the Dale *et al.* (1997a,b) survey of TF distances of clusters to  $cz \simeq 20000 \text{ km s}^{-1}$  is completed.

If we allow the kind of “Hubble bubble” effect claimed by Zehavi *et al.*, our estimate of the uncertainty on *a* would increase somewhat. Because the clusters in our sample straddle the edge of the bubble, the impact of the geocentric flow on *a* is not very large. Given the cluster distance distribution, we estimate that the net shift in the TF template magnitude offset, between a “no geocentric flow” solution and a “Hubble bubble” solution, to amount to less than 0.03 mag. The combination of this contribution with the already quoted uncertainty of 0.05 mag, would raise the error on *a* to 0.06 mag. Zehavi *et al.* have cogently argued that a region of  $70^{-1}$  Mpc radius could be underdense by 20% or so, which

is the amount necessary to produce the suggested local acceleration of the Hubble flow, without stretching too hardly the range of plausibility of the cosmological power spectra. One would be left, of course, with the nagging coincidence of the central location of the LG in the void. But non-conspiratorial coincidences do occur.

If the LG were to be near the center of a “Hubble bubble”, dipole solutions would not be affected, whether the bubble effect were to be maintained in the data or removed by the exclusion of geocentric solutions. The peculiar velocities measured for individual clusters, on the other hand would differ in the two scenarios: the exclusion of geocentric solutions would reduce the peculiar velocity estimates, producing a somewhat more quiescent picture of the kinematic fluctuations. In the remainder of this paper, we will carry out calculations using the peculiar velocities as listed in Table 1. When applicable, the effect of a “Hubble bubble” on our results will be estimated and discussed.

#### 4. The Global Motion of Supercluster Structures

Our cluster sample yields interesting information on the global motion of three large-scale structures: the Perseus–Pisces, Coma and Hydra–Centaurus superclusters. The two main clusters in the Coma region, A1367 and A1656, both have small peculiar velocities which average to about  $+150 \text{ km s}^{-1}$ ; within one-sigma, the global motion of the supercluster with respect to the CMB reference frame is nil.

The two Pisces groups (N383 and N507) and A262 in the Perseus–Pisces supercluster also exhibit a similar pattern: none has a large amplitude  $V_{pec}$  and the average of their motions is about  $75 \text{ km s}^{-1}$ ; within one-sigma, the global motion of the supercluster is again nil. It has been claimed (Willick 1990) that Perseus–Pisces as a whole has a large negative velocity, on the order of  $-400 \text{ km s}^{-1}$  in the CMB reference frame; this is of comparable amplitude to the velocity of infall of the LG towards the GA region, suggesting that both the LG and Perseus–Pisces are ‘travel companions’ in their infall towards a structure much more distant than Hydra–Centaurus (Scaramella *et al.* 1989). Our results indicate that the denser regions in the Perseus–Pisces supercluster do not have a global motion as large as  $400 \text{ km s}^{-1}$  with respect to the CMB, at the better than 99% confidence level, and therefore that the region between the LG and the Perseus–Pisces supercluster is affected by a relatively steep peculiar velocity gradient.

The GA region, intended loosely as the conglomerate of groups and clusters which includes Antlia, N3557, Cen30, Hydra, ESO 508 and A3574 among objects in our sample, presents a more complex picture. It lacks a clear, large amplitude central structure

and it stretches in  $cz_{tf}$  between 2500 and 5000  $\text{km s}^{-1}$ . The cluster A3627, located at  $(l, b) = 325^\circ, -7^\circ$  at  $cz \simeq 4300 \text{ km s}^{-1}$  and studied by Kraan–Korteweg *et al.* (1996), is at too low a galactic latitude to permit the accurate photometry required by TF work. The foreground structures, Antlia, ESO508 and Cen30, exhibit significant outflow (positive) velocities, while the two structures in the background, A3574 and more significantly Hydra, exhibit backflow (negative) velocities. The large amplitude of the velocities of several of the clusters, between 200 and 450  $\text{km s}^{-1}$ , are significant at the 2–3–sigma level. While the evidence of the motion of Hydra and A3574 alone may be statistically too sparse to allow a claim of backflow in the GA region, it tends to corroborate rather than refute the early claim of Dressler & Faber (1990). The observation of a negative velocity for Hydra suggests that the early suggestion of Shaya (1984) and Tammann & Sandage (1985), that centered the successively named GA no farther than Hydra–Centaurus, may be correct. Overall, the scenario that emerges from the data in Table 1 is one where the large–scale structures in the local universe exhibit very little global deviation from smooth Hubble flow.

## 5. Completeness of the Cluster Sample

Our cluster sample is not a fair sample of the local universe. At low redshifts it includes several groups of low enough richness so that they do not meet criteria for inclusion in the Abell/ACO catalogs. Beyond  $cz \sim 6000 \text{ km s}^{-1}$ , the majority of Abell/ACO clusters are not included in our sample. Figure 2 shows a redshift histogram of our cluster sample vis–a–vis with that of the members of the Abell catalog. Between  $cz \simeq 2000 \text{ km s}^{-1}$  and  $cz \sim 9000 \text{ km s}^{-1}$ , the selection function  $s(cz)$ , i.e. the probability of a given Abell/ACO cluster to be included in our sample, drops roughly in proportion to  $e^{-(cz/2300)}$ . Only one in ten Abell clusters with  $cz$  between 7000 and 9500  $\text{km s}^{-1}$  enters our sample. The steepness of the selection function has an impact on the kinematical inferences discussed in this paper. For example, the estimate of bulk flows in the peculiar velocity field, and especially its comparison with the results of cosmological simulations, generally refers to the global motion of the matter within a region bounded by a top hat or a Gaussian filter, more frequently the former. In an observed sample such as ours, it would then be necessary to assign higher weight to distant clusters, roughly by a factor proportional to the inverse of the selection function, in order to obtain estimates not inordinately affected by the characteristics of the very local peculiar velocity field. This form of weighting increases the uncertainty of derived dipoles, because the peculiar velocity of clusters is known with an accuracy  $\epsilon_v$  which is roughly of the order of 4% of their  $cz_{tf}$ . In an volume–weighted measure of the peculiar velocity dipole or bulk flow, each object should be weighted according to  $(s\epsilon_v^2)^{-1}$ , which in our case turns out to be a roughly constant value between

2000 and 9000 km s<sup>-1</sup>, the redshift stretch of our cluster sample. In other words, the computation of a bulk flow or a dipole using *equal weights* for distant and nearby clusters approximates filtering the peculiar velocity field by a top hat of radius equal to the redshift range of our data.

## 6. The Cluster Peculiar Velocity Distribution Function

It is of interest to know the distribution function of peculiar velocities of clusters. Such function can provide an indication of the variance in the peculiar velocity field, and it can be directly compared with numerical simulations obtained within the framework of different cosmological models, thus providing an observational test for their adequacy. Before we proceed to an estimate of the distribution function, we touch the problem of Malmquist bias on peculiar velocity measurements.

Statistical underestimates of TF distances arise due to the Malmquist bias, a well-known effect which results from the fact that distance measurements are uncertain and that within a given solid angle the number of possible targets with distance between  $r$  and  $r + dr$  usually increases with  $r$ . Thus, for a set of targets of estimated distance modulus  $\mu_e \pm \epsilon_\mu$  the most probable distance is not  $r_e = 10^{0.2(\mu_e - c)}$  (where  $c$  is the usual scaling term that depends on the adopted units of distance), but a value  $r > r_e$ , because the distribution of targets is such that there is a larger number of them between  $\mu_e$  and  $\mu_e + \epsilon_\mu$  than between  $\mu_e$  and  $\mu_e - \epsilon_\mu$ . When the assumption is made that the targets are distributed in space in Poisson form, the effect is referred to as the “homogeneous Malmquist bias” (HMB). In that case,

$$r = r_e e^{3.5\Delta^2} \quad \text{where} \quad \Delta = 10^{0.2\epsilon_\mu} - 1 \quad (6)$$

$\Delta$  is the relative distance error. When the targets are individual galaxies, the TF relation yields distance moduli with an uncertainty on the order of  $\epsilon_\mu \simeq 0.3$  mag, which translates in a HMB correction  $r/r_e \simeq 1.08$ . For clusters, the uncertainty  $\epsilon_\mu$  is significantly reduced, and  $r/r_e$  is closer to 1.01.

The HMB modifies the TF distances  $cz_{tf}$  in columns 7 and 9 of Table 1 to  $cz_{tf}|_{mb}$ , as shown in Equation (6), where the errors  $\epsilon_\mu$  are those listed in columns 2 and 3 of Table 1. The peculiar velocities are thus modified from the values listed in Table 1 to  $V_{pec}|_{mb} = cz - cz_{tf}|_{mb}$ . The corrections are generally small, except for the most distant clusters or those with large  $\epsilon_\mu$ . We use such modified values in the estimate of the distribution function of peculiar velocities of clusters, but for simplicity we will forego carrying the clumsy *mb* subscript. Since the distribution of clusters in space is not Poissonian, the bias correction should in principle take into account the clustering

characteristics of the distribution. However, since the corrections are small, the cluster population is quite sparse and an inhomogeneous correction is difficult to estimate and thus highly uncertain, the correction for a simple HMB is deemed sufficient for our purposes. In fact, both in the computation of the peculiar velocity distribution function, presented in the remainder of this section, and in that of dipoles, as described in the next section, the Malmquist bias correction has very little impact on the final results.

We have only access to one component of a cluster’s peculiar velocity, that along the line of sight. In addition, as indicated in Table 1, that value is generally known with a significant amount of uncertainty. In Figure 3, we graphically present the values and uncertainties of the peculiar velocities of the 24 clusters in our sample. The cluster peculiar velocities (for the **in+** samples) are represented by Gaussian functions of equal area  $A_i \exp[-(V_{pec,1d} - V_{pec,i})^2/2\epsilon_{v,i}^2]$  (where the amplitudes  $A_i \propto \epsilon_{v,i}^{-1}$ ), centered at the value of  $V_{pec,i}$  for the  $i$ -th cluster, and with dispersion equal to the error on  $V_{pec,i}$ ,  $\epsilon_{v,i}$ . The sum of those yields the observed distribution function  $f_{obs}(V_{pec,1d})$  of the line-of-sight peculiar velocity values, measured in the CMB reference frame, as broadened by observational errors (heavy line in Figure 3, arbitrarily rescaled). The distribution is slightly asymmetric, due to the large velocities of nearby groups, such as Ursa Major and Eridanus. Note that  $V_{pec} = 0$  is defined by setting the monopole of clusters farther than 4000 km s<sup>-1</sup> to zero, as discussed in Section 3. A Gaussian fit with zero mean to  $f_{obs}(V_{pec,1d})$  yields a dispersion  $\sigma_{1d,obs} = 325 \pm 54$  km s<sup>-1</sup>. The uncertainty can be estimated from the nominal errors of the fit or, alternatively, by Monte Carlo simulations of synthetic data sets. The simulations are obtained by producing data sets where the peculiar velocity of the  $i$ -th cluster is a random deviate of  $A_i \exp[-(V_{pec,1d} - V_{pec,i})^2/2\epsilon_{v,i}^2]$ . Each simulation of a cluster set is fit and the scatter among fitted values of  $\sigma_{1d,obs}$  yields the uncertainty. The two estimates of error agree. Since the observed distribution function is broadened by errors,  $\sigma_{1d,obs}$  overestimates the true dispersion. The broadening produced by the varied combination of error functions is easily calculated by Monte Carlo simulations, yielding a dispersion corrected for error broadening  $\sigma_{1d} = 270 \pm 54$  km s<sup>-1</sup>. These figures apply to the **in+** samples. Repeating the same exercise for the peculiar velocities obtained from the **in** samples, we obtain  $\sigma_{1d,obs} = 375$  km s<sup>-1</sup> and  $\sigma_{1d} = 277 \pm 63$  km s<sup>-1</sup>, respectively.

What would be the effect of a Zehavi *et al.* (1998) Hubble bubble on our estimate of  $\sigma_{1d}$ ? We gauge it by allowing for an acceleration of the Hubble flow by 6% within  $cz \sim 7000$  km s<sup>-1</sup>; we then estimate the shift in the kinematical zero point resulting from this assumption, with respect to that obtained if nil net flow for the clusters between 4000 and 9500 km s<sup>-1</sup> is assumed (which led to the peculiar velocities in Table 1). We correct the peculiar velocities by the zero point shift and repeat the calculations described in the previous paragraph. The inclusion of a Hubble bubble broadens  $\sigma_{1d}$  by 45 km s<sup>-1</sup>.

While the exclusion of large-scale geocentric flows may bias our estimate of  $\sigma_{1d}$  low, the presence in our sample of poor groups at low redshift (Ursa Major, Eridanus, MDL59) may have the effect of biasing the result on the high side. Nearby groups have among the largest observed peculiar velocities, which may be representative of locations in the peripheral parts of superclusters, regions characterized by high, large-scale density gradients. Rich clusters tend to reside in the denser parts of superclusters, near the bottom of gravitational potential wells, and the variance in their motions may be more subdued.

Thus, allowing for uncertainties on systematic biases associated with a possible geocentric deviation from Hubble flow of a few percent and for the presence of small foreground groups in our sample, it appears that the cosmic variance in the 1-d peculiar velocity of clusters in the local universe can be well approximated by a r.m.s. value of the order of

$$\sigma_{1d} = 300 \pm 80 \quad \text{kms}^{-1} \quad (7)$$

This number is in good agreement with previous estimates by Bahcall & Oh (1996) and by Watkins (1997), based on our data, and is significantly lower than values obtained from previous measurements of cluster velocities (e.g. Mould *et al.* 1991), which were affected by much larger errors than those associated with this set. Bahcall and Oh (1996) and Borgani *et al.* (1997), compared the cluster peculiar distribution function obtained from these data with numerical simulations in the framework of different cosmological models, finding support in these data for models with relatively low values of  $\Omega$ .

## 7. Dipoles of the Cluster Peculiar Velocity Field

### 7.1. Procedures

Although few in number, the distance moduli of the clusters in our sample are determined with a high degree of accuracy, on the order of 0.08 magnitudes, or 4% of  $cz_{tf}$ . As a result, a good estimate is possible of the low order spherical harmonics of their peculiar velocity field, namely the dipole. We only measure the line of sight component of the peculiar velocity, thus the problem reduces to computing the dipole of a scalar field. Since we are interested in the comparison with  $\mathbf{V}_{cmb}$  and  $\mathbf{V}_{lp}$ , the apparent motions of the LG with respect to, respectively, the CMB and the Lauer & Postman cluster reference frames, we shall estimate the dipole of the *reflex* motion of the LG with respect to our cluster set. If  $-V_i$  is the peculiar velocity of the  $i$ -th cluster *in the LG reference frame*, and  $\epsilon_i$  is the uncertainty on that quantity, we solve for the vector  $\mathbf{V}_d$  of the dipole moment by

minimizing the merit function

$$\chi^2 = \sum_i \frac{1}{s_i} \left( \frac{V_i - \mathbf{V}_d \cdot \hat{\mathbf{r}}_i}{\epsilon_i} \right)^2 \quad (8)$$

where  $\hat{\mathbf{r}}_i$  is the unit vector in the direction of the  $i$ -th cluster and  $s_i$  is the selection function at its distance. The errors of a dipole solution based on a small number of samples  $N_c$  can be capriciously distributed. We thus obtain an error estimate of our results by producing a large number  $N_{sets}$  of synthetic data sets, and monitoring the scatter among the resulting dipole solutions. Each synthetic cluster set is obtained as follows: the locations of the clusters,  $[\hat{\mathbf{r}}_i]$ , are maintained as observed but the peculiar velocity of each cluster is extracted as a random deviate from a Gaussian of center  $-V_i$  and dispersion  $\epsilon_i$ . In our simulations,  $N_{sets} = 1000$ . The error ellipsoid of the components of the dipole solution of the observed cluster set is estimated from the scatter among the  $N_{sets}$  dipole solutions for the synthetic cluster sets.

As discussed in Section 5, our cluster set is not a fair sample. Nearby clusters are more likely to be part of the set than distant ones. An estimate of the peculiar velocity dipole moment that does not take into consideration the selection function of the sample will thus heavily weigh the nearby clusters over the more distant ones. As a function of distance, the shape of the selection function  $s$  and the lognormal character of the peculiar velocity errors do however combine in such a way that if each cluster’s contribution to the dipole is weighed inversely proportional to the sample selection function, as in Equation (8), the product  $s_i \epsilon_i^2$  is roughly constant. An alternative technique to correcting for the fading of the sample at higher redshifts is that of assigning a weight to each cluster which is proportional to  $r_n^3$ , where  $r_n$  is the distance to the  $n$ -th nearest neighbor in the sample and  $n$  is usually a number selected between 3 and 9. For a small sample such as ours, this form of volume-weighting introduces a substantial measure of erratic behavior, and for the purpose of approximating top hat volume-weighting, we adopt the simpler approach of using unit weights  $s_i \epsilon_i^2$ .

Below, we present dipole solutions using  $(s_i) \equiv 1$ , which give large weight to nearby clusters (columns labeled ‘Case  $a$ ’ in Table 2), and  $(s_i \epsilon_i^2) \equiv 1$ , which is equivalent to weighing each cluster in proportion inverse to the selection function discussed in Section 5 (columns labeled ‘Case  $b$ ’ in Table 2). The second approach increases the effective depth of the solution, at the cost of increased noise.

Equation (8) is solved for the three Cartesian components of  $\mathbf{V}_d$ , directed respectively towards the Galactic Center,  $(l, b) = (90^\circ, 0^\circ)$  and the  $b = 90^\circ$ . The amplitudes of the dipoles listed in Table 2 are corrected for the “error bias”, i.e.  $|\mathbf{V}_d|^2 = V_{dx}^2 + V_{dy}^2 + V_{dz}^2 - e_x^2 - e_y^2 - e_z^2$ , where  $e_x, e_y, e_z$  are the uncertainties on the Cartesian coordinates of the dipole.



Table 2. Cluster Dipole Solutions

| Set                                           | $N_c$ | Case <i>a</i> :         | $s_i \equiv 1$               | Case <i>b</i> :         | $s_i \epsilon_i^2 \equiv 1$  |
|-----------------------------------------------|-------|-------------------------|------------------------------|-------------------------|------------------------------|
|                                               |       | V<br>km s <sup>-1</sup> | ( <i>l</i> , <i>b</i> )<br>° | V<br>km s <sup>-1</sup> | ( <i>l</i> , <i>b</i> )<br>° |
| 1. All                                        | 24    | 759±083                 | (229,+31)±11                 | 450±141                 | (266,+31)±26                 |
| 2. All ZOA $\bar{V}_{pec} = 0$                | 30    | 449±121                 | (234,+43)±28                 | 364±148                 | (272,+38)±31                 |
| 3. All ZOA $\bar{V}_{pec}$ from SF            | 30    | 609±100                 | (240,+36)±18                 | 472±118                 | (266,+26)±22                 |
| 4. $cz_{tf} > 3000$                           | 18    | 611±129                 | (263,+18)±18                 | 496±196                 | (270,+37)±37                 |
| 5. $cz_{tf} > 3000$ ZOA $\bar{V}_{pec} = 0$   | 23    | 447±141                 | (277,+48)±35                 | 433±173                 | (278,+51)±45                 |
| 6. $cz_{tf} > 3000$ ZOA $\bar{V}_{pec}$ (SFI) | 23    | 565±103                 | (268,+22)±17                 | 484±158                 | (271,+38)±30                 |
| 7. $cz_{tf} < 6000$                           | 17    | 794±070                 | (231,+31)±11                 | 543±090                 | (263,+23)±16                 |
| 8. $cz_{tf} < 6000$ ZOA $\bar{V}_{pec} = 0$   | 21    | 469±121                 | (239,+43)±25                 | 433±161                 | (275,+34)±27                 |
| 9. $cz_{tf} < 6000$ ZOA $\bar{V}_{pec}$ (SFI) | 21    | 663±083                 | (239,+36)±17                 | 534±090                 | (268,+19)±16                 |

## 7.2. Dipole Calculation. Filling the Zone of Avoidance

The region of the sky close to the galactic plane, roughly bounded by  $|b| < 20^\circ$ , is not sampled by our cluster set. The effect on the dipole calculations of the ZoA, which amounts to approximately a quarter of the sky, is estimated by relying on the Monte Carlo approach described in the preceding section, of generating a large number of synthetic cluster sets. For a given observed set of  $N_c$  clusters, we produce  $N_{sets}$  of  $1.25N_c$  clusters, where the additional  $0.25N_c$  “cloned” clusters are assigned random coordinates in the ZoA and distances  $cz_{tf}$  which are random deviates of the distribution for the  $N_c$  observed clusters. The assignment of a peculiar velocity to the cloned clusters is approached in two independent ways, providing outer boundaries to the estimate of the effect of ZoA on the uncertainty of the dipole solution:

(i) In the first approach, a peculiar velocity is extracted from a Gaussian distribution of zero mean *with respect to the Local Group*, and dispersion  $\sigma_{1d} = 300 \text{ km s}^{-1}$ . This approach reduces the amplitude of any dipole signal that may be present in the  $N_c$  cluster sample. Assigning a peculiar velocity from a Gaussian distribution of zero mean in the CMB reference frame would be more appropriate, on the basis of the results discussed in Section 6, but it would reinforce the match of the reflex cluster dipole with  $\mathbf{V}_{cmb}$ . The chosen approach, while not producing reliable dipole parameters, will yield an upper limit to the uncertainty of the dipole determination arising from the ZoA undersampling bias.

(ii) In our second approach to estimating the peculiar velocity of a random cluster in the ZoA, we resort to an independent data set of peculiar velocities: that provided by our sample of field late spiral galaxies (SFI; see e.g. Giovanelli *et al.* 1994 for a description of the sample). SFI is slightly less deep than the SCI cluster sample, but it contains a sufficient number of galaxies at  $cz$  near  $9,000 \text{ km s}^{-1}$  for the purposes of this exercise. It includes 680 galaxies with galactic latitudes lower than  $30^\circ$ . Once a ZoA cluster is randomly assigned position  $\hat{\mathbf{r}}_i$  and distance  $cz_{tf,i}$ , SFI galaxies within  $2000 \text{ km s}^{-1}$  of the cluster are selected and ranked by the distance between galaxy  $j$  and the cluster,  $d_j = \sqrt{(cz_{tf,i}\hat{\mathbf{r}}_i - cz_{tf,j}\hat{\mathbf{r}}_j)^2}$ . The cluster is then assigned a peculiar velocity  $v = \sum_j v_j d_j^{-1} / \sum d_j^{-1}$ , where the sum is over the nearest 15 galaxies to cluster  $i$ . This approach preserves the characteristics of the large-scale peculiar velocity field and yields the best possible estimate of the cluster dipole, corrected for the effect of ZoA undersampling.

### 7.3. Dipole Calculation. Results

Table 2 displays values of the apex coordinates of dipole solutions of the reflex motion of the LG with respect to the cluster set, calculated for a variety of subsets and processing options.

Solution sets are computed for three main subsamples: (a) all clusters together (sets 1 through 3); (b) clusters farther than  $cz_{tf} = 3000 \text{ km s}^{-1}$  (sets 4 through 6); (c) clusters within  $cz_{tf} = 6000 \text{ km s}^{-1}$  (sets 7 through 9). Solutions are computed for **in** cluster galaxy samples; the analogous ones for the **in+** samples do not differ in a significant way from those tabulated. Computations are carried out with the following different approaches: without correcting for the undersampling in the ZoA (sets 1, 4, and 7); correcting for the ZoA undersampling by simulating mock clusters with zero mean peculiar velocity with respect to the LG (sets 2, 5 and 8); correcting for the ZoA undersampling by simulating mock clusters of peculiar velocities derived from those of the field (SFI) galaxies in the ZoA neighborhood (sets 3,6 and 9). Furthermore, each solution is computed separately weighing each cluster by setting  $s_i \equiv 1$  (columns 3 and 4, labeled 'Case *a*') and by setting  $s_i \epsilon_i^2 \equiv 1$  (columns 5 and 6, labeled 'Case *b*'). Tabulation of the dipole solutions includes the description of the solution set (col. 1), the number of clusters per solution set (col. 2), the modulus of the dipole vector  $\mathbf{V}_d$  and its apex galactic coordinates (cols. 3, 4 and 5), with estimates of errors. The error estimates were carried out by producing  $N_{sets} = 1000$  synthetic versions of each sample, as discussed in Section 6.2. The solutions we consider the most robust are numbers 3, 6 and 9

Figure 4 displays the apices of some of the solution sets in Table 2, namely those for sets 3, 6 and 9. In each case we display both the *a* (left-hand column) and the *b* solution (right-hand column). On a grid of galactic coordinates centered at  $(l, b) = (180, 0)$ , with  $l$  increasing right to left, we plot the dipole apices of each of the  $N_{sets} = 1000$  synthetic cluster sets corresponding to each sample. Contours at the 63% (one sigma) and 95% (2 sigma) confidence levels are plotted. The dipole solution in each case (the center of those contours) is also entered at the top right of each panel, in the following order: dipole velocity, apex longitude and latitude. The apex of the motion of the LG with respect to the CMB is plotted as a large filled circle, and the apex of the LG motion in the Lauer & Postman solution is plotted as a large, crossed circle.

Figure 5 displays the apices of solution sets 4, 5 and 6, all for the same subsample of clusters with  $cz_{tf} > 3000 \text{ km s}^{-1}$ . This figure illustrates the effect of different approaches to correcting for the undersampling in the ZoA.

We note immediately that the dipole of the LG motion with respect to the various sets

of clusters is in substantial agreement with the CMB solution, while the Lauer & Postman solution is excluded with a high level of confidence. The inclusion of clusters in the ZoA with random peculiar velocities averaging zero, as shown in panels (c) and (d) of Figure 5, increases the uncertainty of the dipole solution and raises its apex to higher positive latitudes. On the other hand, the adoption of synthetic clusters in the ZoA with peculiar velocities as inferred from those of neighboring field galaxies suggests a tightening of the quality of the solution, an indication that both the set of clusters of galaxies and that of field galaxies reflect the same peculiar velocity field.

As indicated in Table 1, nearby clusters exhibit relatively large peculiar velocities with respect to the CMB, sharing that characteristic with the LG. Their exclusion, as shown in panels (c) and (d) of Figure 4, thus yields dipole solutions that approach even more closely the CMB solution. While the uncertainties are larger for solutions 4–6, they suggest that *the dipole moment of the LG motion with respect to clusters at  $cz_{tf} > 3000 \text{ km s}^{-1}$  matches well the CMB dipole; this result is consistent with the assumption that, as a whole and apart from solutions which are purely geocentric, that set of clusters is at rest with respect to the CMB.* This result is in good agreement with an analogous study carried out using field spirals (Giovanelli *et al.* 1998), which yields strong indication for the fact that at distances on the order of 5–6000  $\text{km s}^{-1}$ , convergence appears to have been achieved. Given the magnitude of the uncertainties displayed in Table 2, it is however fair to say that the cluster data set alone leaves room for the possibility that up to one-third of  $\mathbf{V}_{cmb}$  arising outside the volume subtended by the cluster sample. The field galaxy sample does however pose tighter constraints, and we are inclined to believe that the combined evidence of field and cluster dipoles establishes a good case for convergence within 9000  $\text{km s}^{-1}$ .

In Figure 6, we plot all the dipole solutions listed in Table 2 in two of three possible stereographic projections, i.e. in  $(l, b)$  and  $(|\mathbf{V}_d|, b)$ , approximated as Cartesian coordinates. The CMB dipole is plotted as a filled circle and the Lauer & Postman solution of the LG dipole as a crossed circle.

#### 7.4. Bulk Flows

The difference  $(\mathbf{V}_{cmb} - \mathbf{V}_d)$  for any of the solutions in Table 2 yields the bulk flow motion of the corresponding sample with respect to the CMB. Because many of the cluster dipole solutions match so closely the CMB dipole, resulting bulk flows are quite modest, and their directions largely unconstrained. The most robust estimates of the bulk flow for the total cluster sample is  $310 \pm 120 \text{ km s}^{-1}$ , towards  $(337^\circ, -15^\circ) \pm 23^\circ$  (Case *a*) and  $151 \pm 120 \text{ km s}^{-1}$ , towards  $(295^\circ, +28^\circ) \pm 45^\circ$  (Case *b*), values which are obtained

for solution 3. For solution 6 of the  $cz_{tf} > 3000 \text{ km s}^{-1}$  subsample, the bulk flow is not significant for case ‘a’ and a barely marginal  $165 \pm 150$  towards  $(278^\circ, -7^\circ) \pm 45^\circ$  for case ‘b’. For solution 9 of the  $cz_{tf} < 6000 \text{ km s}^{-1}$  subsample, the two bulk flow solutions are respectively  $336 \pm 144 \text{ km s}^{-1}$ , towards  $(348^\circ, -20^\circ) \pm 25^\circ$  and a marginal  $131 \pm 90 \text{ km s}^{-1}$ , towards  $(325^\circ, +62^\circ) \pm 60^\circ$ . At the 95% confidence level or better, these data exclude the existence of a bulk flow of amplitude  $350 \text{ km s}^{-1}$  or larger, centered on the LG, involving the equal volume-weighted contents of a sphere of  $6000 \text{ km s}^{-1}$  radius, or of the contents of a spherical shell of radius between 3000 and  $-9000 \text{ km s}^{-1}$ .

## 8. Summary

We have analyzed the peculiar velocity field as described by a set of 24 clusters and groups of galaxies at  $cz$  between 1000 and  $9200 \text{ km s}^{-1}$ . The following results emerge from our study:

- The peculiar velocity field as outlined by these objects is rather quiescent. No velocities in excess of  $600 \text{ km s}^{-1}$ , with respect to the CMB reference frame, are observed. This is in marked contrast with previous results.
- The main supercluster structures within the reach of the sample, such as the Coma supercluster and the Pisces–Perseus supercluster, exhibit global deviations from Hubble flow in the CMB reference frame that cannot be distinguished from null, with uncertainties of less than  $150 \text{ km s}^{-1}$ . Global flows of those structures at velocities in excess of  $400 \text{ km s}^{-1}$  can be excluded at the 99% confidence level.
- The dispersion of the line-of-sight peculiar velocity distribution function of clusters, as measured in the CMB reference frame, is  $\sigma_{1d} = 300 \pm 80 \text{ km s}^{-1}$ .
- We do not find evidence of a ‘Hubble bubble’, i.e. a geocentric deviation from Hubble flow with amplitude of 6.6% within  $cz \sim 7000 \text{ km s}^{-1}$ , as reported by Zehavi *et al.* (1998). Our sample does however barely straddle the edge of the bubble and has low statistical significance. We can thus neither corroborate nor refute the Zehavi *et al.* result.
- The dipole of the reflex motion of the LG with respect to the cluster set approaches closely the vector of the CMB dipole. When the dipole is computed with respect to the clusters that are farther than  $cz \sim 3000 \text{ km s}^{-1}$ , the two coincide within the errors. This result suggests that the convergence depth of the local universe is largely approached within the limits of the cluster sample, i.e. the more distant clusters in our sample populate a shell globally at rest with respect to the CMB. The cluster set alone is however insufficient to

exclude that up to  $1/3$  of  $\mathbf{V}_{cmb}$  may arise outside the volume subtended by the sample. A parallel study which uses field spirals is in agreement with the cluster data and reinforces the indication of convergence within  $6\text{--}9000 \text{ km s}^{-1}$ .

- The Lauer & Postman dipole solution is excluded as possible by our data at better than the 99% confidence level. The bulk flow of the contents of a sphere of radius  $6000 \text{ km s}^{-1}$ , centered on the LG, is small. Its amplitude is less than  $300 \text{ km s}^{-1}$  and its poorly constrained apex is in the general direction of  $l = 320^\circ$ .

The results presented in this paper are based on observations carried out at the Arecibo Observatory, which is part of the National Astronomy and Ionosphere Center (NAIC), at Green Bank, which is part of the National Radio Astronomy Observatory (NRAO), at the Kitt Peak National Observatory (KPNO), the Cerro Tololo Interamerican Observatory (CTIO), the Palomar Observatory (PO), the Observatory of Paris at Nançay and the Michigan–Dartmouth–MIT Observatory (MDM). NAIC is operated by Cornell University, NRAO by Associated Universities, Inc., KPNO and CTIO by Associated Universities for Research in Astronomy, all under cooperative agreements with the National Science Foundation. The MDM Observatory is jointly operated by the University of Michigan, Dartmouth College and the Massachusetts Institute of Technology on Kitt Peak mountain, Arizona. The Hale telescope at the PO is operated by the California Institute of Technology under a cooperative agreement with Cornell University and the Jet Propulsion Laboratory. This research was supported by NSF grants AST94–20505 and AST96–17069 to RG, AST95–28860 to MH and AST93–47714 to GW.

## REFERENCES

- Bahcall, N.A. and Oh, S.P. 1996, ApJ 462, L49
- Borgani, S., da Costa, L.N., Giovanelli, R., Haynes, M.P., Salzer, J.J. & Wegner, G. 1997, ApJ 482, 121
- Branchini, E. et al. 1996, ApJ 461, L17
- da Costa, L.N., Freudling, L.N., Wegner, G., Giovanelli, R., Haynes, M.P. and Salzer, J.J. 1996, ApJ 468, L5
- Dale, D.A., Giovanelli, R., Haynes, M.P., Hardy, E. & Campusano, L. 1997a, AJ 114, 455
- Dale, D.A., Giovanelli, R., Haynes, M.P., Hardy, E. & Campusano, L. 1997b, AJ 115, 418
- Dekel, A. 1994, ARA&A 32, 371
- de Vaucouleurs, G., de Vaucouleurs, A. & Corwin, H.G. 1976, *Second Reference Catalog of Bright Galaxies*, U. of Texas Press, Austin.
- Dressler, A. & Faber, S.M. 1990, ApJ 354, L45
- Giovanelli, R., Haynes, M.P., Salzer, J.J., Wegner, G., da Costa, L.N. and Freudling, W. 1994, AJ 107, 2036
- Giovanelli, R., Haynes, M.P., Wegner, G., da Costa, L.N., Freudling, W. and Salzer, J.J. 1996, ApJ 464, L99
- Giovanelli, R., Haynes, M.P., Herter, T., Vogt, N.P., da Costa, L.N., Freudling, W., Salzer, J.J. and Wegner, G. 1997a, AJ 113, 22 (Paper VI)
- Giovanelli, R., Haynes, M.P., Herter, T., Vogt, N.P., da Costa, L.N., Freudling, W., Salzer, J.J. and Wegner, G. 1997b, AJ 113, 53 (Paper VII)
- Giovanelli, R., Haynes, M.P., Freudling, W., da Costa, L.N., Salzer, J.J. & Wegner, G. 1998, preprint
- Guzzo, L. 1998, *New Astronomy* 2, 517
- Hudson, M. 1993, MNRAS 265, 72.
- Jerjen, H. & Tammann, G.A. 1993, A&A 273, 354

- Kraan–Korteweg, R.C. & Woudt, P.A., Cayatte, V., Fairall, A.P., Balkowski, C. & Henning, P.A. 1996, *Nature* 379, 519
- Lauer, T.R. & Postman, M. 1994, *ApJ* 425, 418
- Lineweaver, C.H., Tenorio, L., Smoot, G.F., Keegstra, P., Banday, A.J. and Lubin, P. 1996, *ApJ* 470, 38
- Lynden–Bell, D. et al. 1988, *ApJ* 326, 19
- Lynden–Bell, D. & Lahav, O. 1988, in *Large–Scale Motions in the Universe: A Vatican Study Week*, ed. by V.C. Rubin and G.V. Coyne, S.J., Princeton U. Press, Princeton, p. 199.
- Malmquist, K.G. 1924, *Medd. Lund Astron. Obs. Ser. II No. 32*, 64
- Mathewson, D.S., Ford, V.L. and Buchhorn, M. 1992, *ApJ* 389, L5
- Mould, J.R., Staveley–Smith, L., Schommer, R.A., Bothun, G.D., Hall, P.J., Han, M.S., Huchra, J.P., Roth, J., Walsh, W. & Wright, A.E. 1991, *ApJ* 383, 467
- Pietronero, L., Montuori, M. & Sylos–Labini, F. 1997, in *Critical Dialogues in Cosmology*, ed. by N. Turok, Singapore:World Publishing, p. 24.
- Riess, A. G., Press, W.H. & Kirshner, R.P. 1995, *ApJ* 445, L91
- Rubin, V.C., Ford, W.K. Jr, Thonnard, N., Roberts, M.S. & Graham, J.A. 1976, *AJ* 81, 719
- Scaramella, R. et al. 1989, *Nature* 338, 562
- Scaramella, R., Vettolani, G. & Zamorani, G. 1994, *ApJ* 422, 1
- Scodeggio, M., Giovanelli, R. and Haynes, M.P. 1997, *ApJ* 113, 101
- Scodeggio, M., Giovanelli, R. and Haynes, M.P. 1998, *AJ* submitted
- Scodeggio, M. 1997, Ph. D. Thesis, Cornell University.
- Shaya, E.J. 1984, *ApJ* 280, 470
- Strauss, M.A., Yahil, A., Davis, M., Huchra, J.P. & Fisher, K.B. 1992, *ApJ* 397, 395
- Tammann, G. and Sandage, A. 1985, *ApJ* 294, 81



Tini–Brunozzi, P. et al. 1995, MNRAS 277, 1210

Tully, R.B. and Fisher, J.R. 1977, A&A 54, 661

Watkins, R. 1997, MNRAS 292, L59

Willick, J.A. 1990, ApJ 351, L5

Yahil, A., Sandage, A. & Tammann, G.A. 1977, ApJ 217, 903

Zehavi, I., Riess, A.G., Kirshner, R.P. & Dekel, A. 1998, preprint astro-ph/9802252

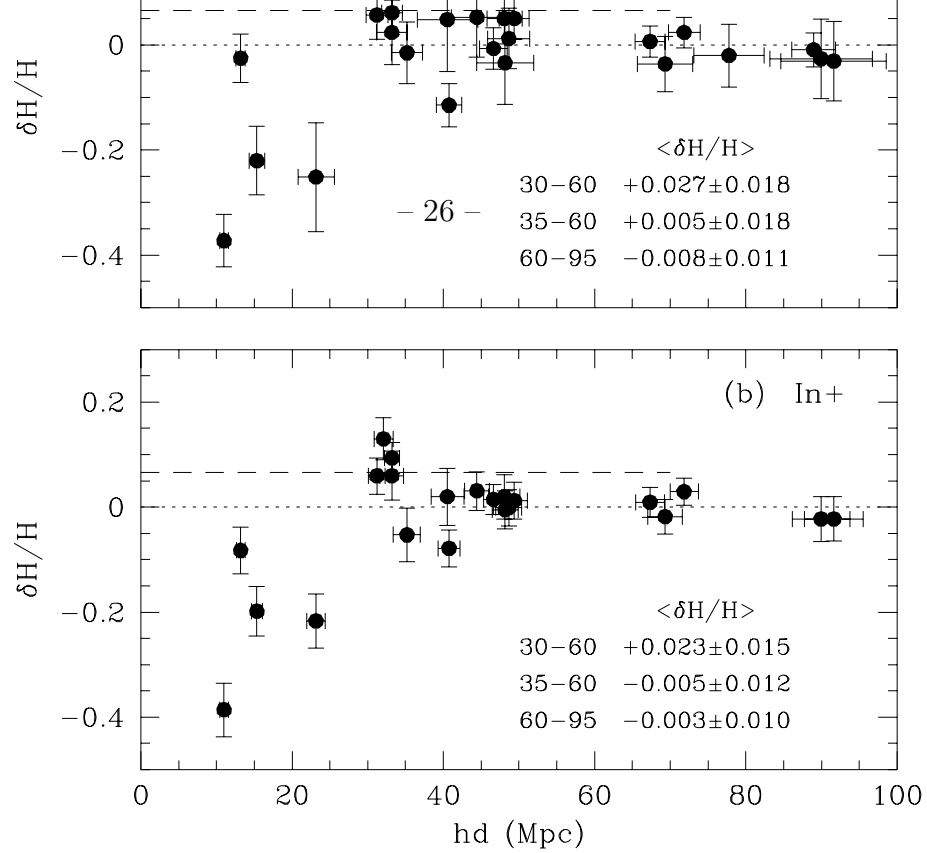


Fig. 1.— Deviations from Hubble flow plotted versus TF distance for the clusters listed in Table 1, separately for the **in** (panel *a*) and for the **in+** (panel *b*) samples. The horizontal dashed lines identify the acceleration of 6.6% in the Hubble flow within  $hd = 70$  Mpc claimed by Zehavi *et al.* (1998). Average values of  $\delta H/H$  are inset for three different windows in  $hd$ .

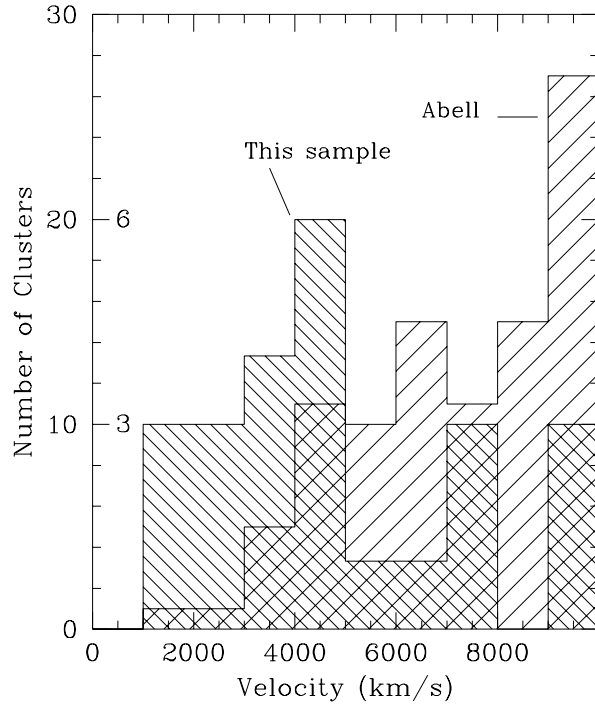


Fig. 2.— Histograms of the number of clusters in our sample *vis-a-vis* that in the Abell cluster catalog. The outer vertical scale applies to the latter, the inner one to the former.

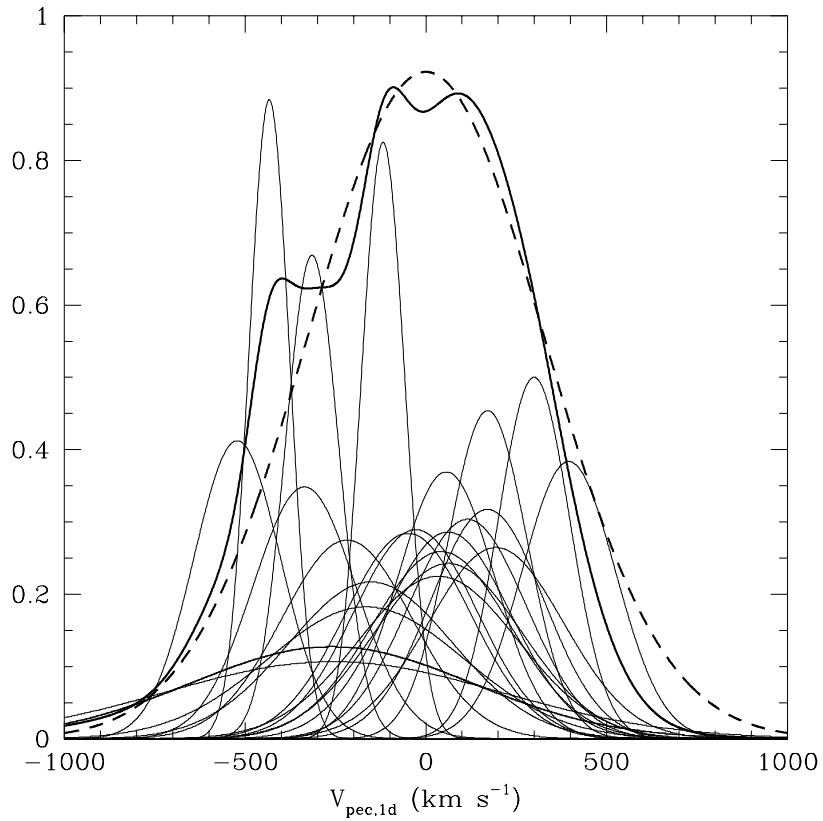


Fig. 3.— Line-of sight peculiar velocities, measured in the CMB reference frame, for the **in+** samples of each cluster listed in Table 1, plotted as equal area Gaussians of dispersion equal to the uncertainty on each measured peculiar velocity. The heavy-trace line is a scaled sum of the individual Gaussians. The dashed line is a Gaussian of dispersion  $325 \text{ km s}^{-1}$ .

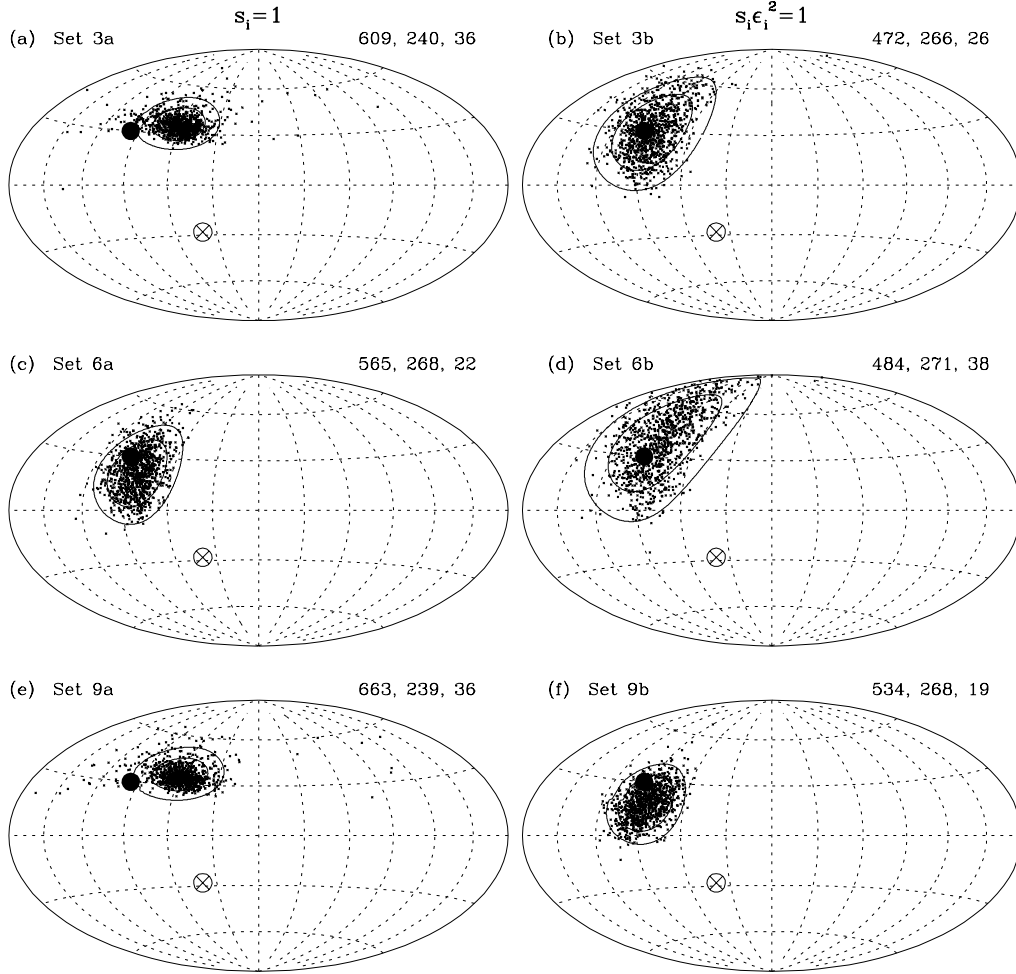


Fig. 4.— Dipole solutions of  $N_{sets} = 1000$  synthetic data sets with the characteristics of solutions 3, 6 and 9 of Table 2. The coordinates of the Aitoff projections are galactic, centered at  $(l, b) = (180^\circ, 0^\circ)$ . The left-hand side panels correspond to solutions estimated with weights as in approach (i) in Section 7.2), while in right-hand panels weights are as in approach (ii) in Section 7.2. The number of the solution on top left of each panel refers to the line number in Table 2. The three numbers on top right of each panel are the amplitude, longitude and latitude of the dipole apex. The large, filled circle in each plot identifies the apex of the CMB dipole, and the apex of the LG motion in the Lauer & Postman solution is plotted as a large, crossed circle.

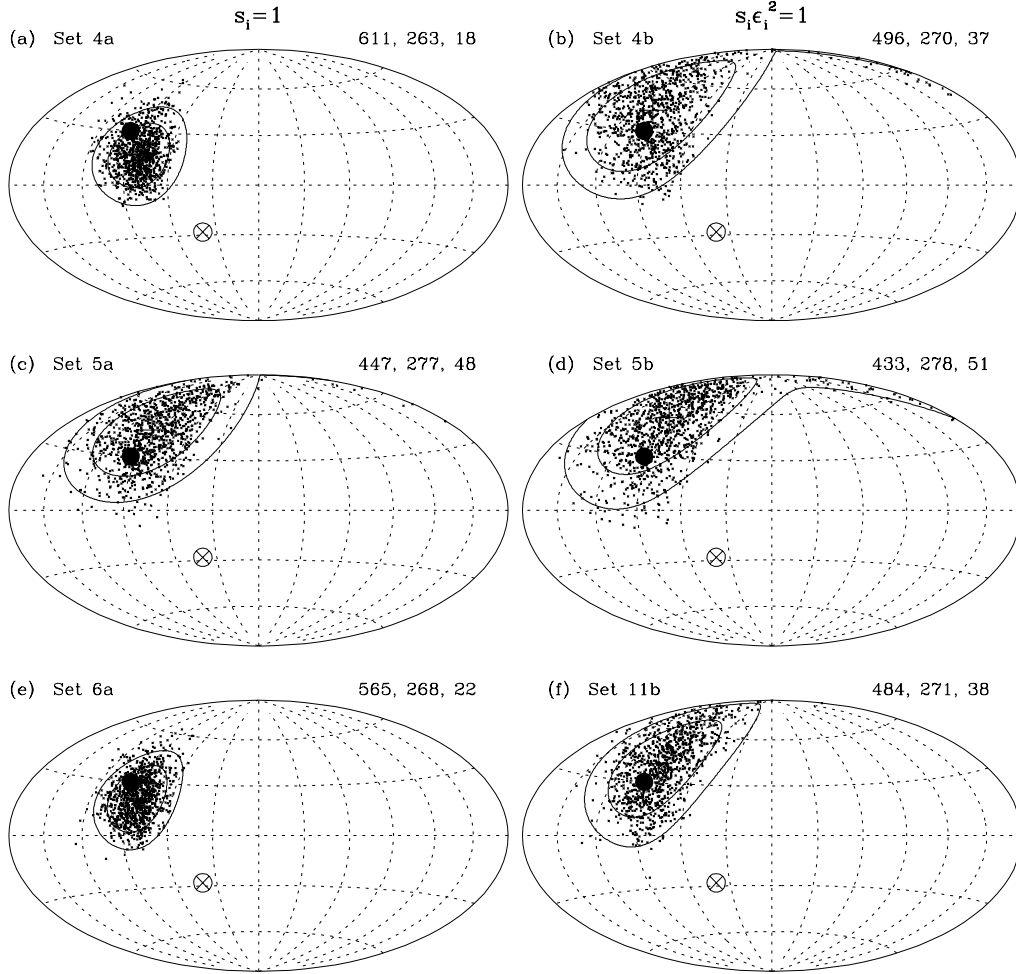


Fig. 5.— Dipole solutions of  $N_{sets} = 1000$  synthetic data sets with the characteristics of solutions 4, 5 and 6 of Table 2. The coordinates of the Aitoff projections are galactic, centered at  $(l, b) = (180^\circ, 0^\circ)$ . The left-hand side panels correspond to solutions estimated with weights as in approach (i) in Section 7.2), while in right-hand panels weights are as in approach (ii) in Section 7.2. The number of the solution on top left of each panel refers to the line number in Table 2. The three numbers on top right of each panel are the amplitude, longitude and latitude of the dipole apex. The large, filled circle in each plot identifies the apex of the CMB dipole, and the apex of the LG motion in the Lauer & Postman solution is plotted as a large, crossed circle.

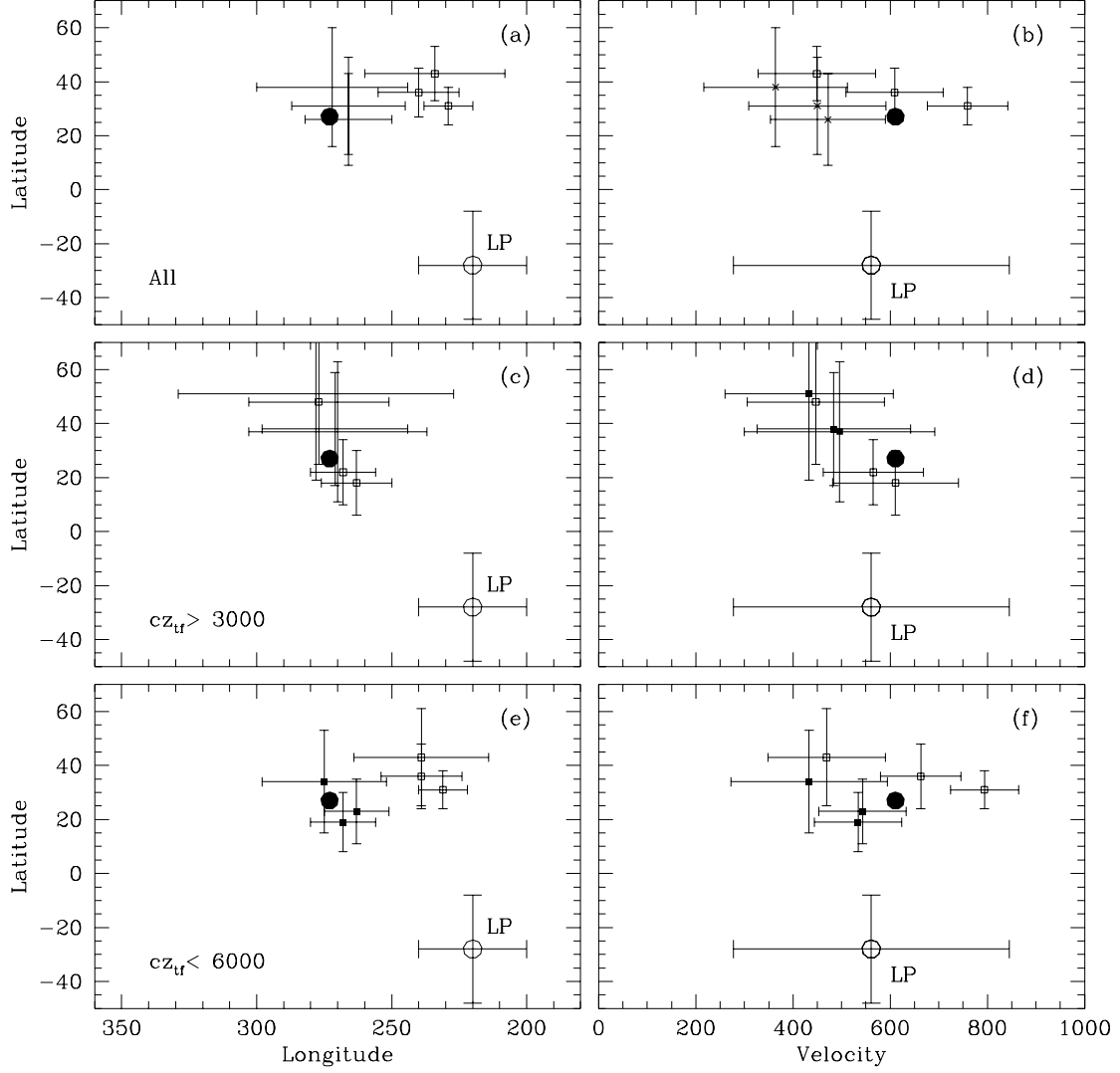


Fig. 6.— Dipole solutions listed in Table 2 are shown as plain error bars, in pairs of stereographic displays in  $(l, b, |\mathbf{V}_d|)$ , respectively for sets 1–3 (panels a and b), 4–6 (panels c and d) and sets 7–9 (panels e and f). Solutions of type ‘a’, estimated by setting  $s_i \equiv 1$ , are plotted as small unfilled squares, while those of type ‘b’, estimated by setting  $s_i \epsilon_v^2 \equiv 1$ , are plotted as filled squares. The large filled circle is the CMB dipole and the crossed circle is the Lauer & Postman dipole solution.